Electronic Supplementary Material (ESI) for Journal of Materials Chemistry C.

Supporting Information

Correlating chemical structure and charge transport ability of dibenzofulvene-based hole transporting materials for stable perovskite solar cells

M. Leoncini[1,2], A.-L. Capodilupo[1,*], D. Altamura[3], C. Giannini[3], G. Accorsi[1], E. Fabiano[4,5], A. Rizzo[1], G. Gigli[1,2], S. Gambino[1,*]

[1] CNR NANOTEC – Istituto di Nanotecnologia, c/o Campus Ecotekne, Via Monteroni, 73100 Lecce, Italy
[2] Dipartimento di Matematica e Fisica "E. De Giorgi", Università del Salento, c/o Campus Ecotekne, via Arnesano, 73100 Lecce, Italy
[3] CNR IC – Istituto di Cristallografia, via Amendola 122/O, 70126, Bari, Italy.
[4] CNR IMM – Istituto di Microelettronica e Microsistemi, c/o Campus Ecotekne, Via Monteroni, 73100, Lecce, Italy
[5] IIT - Istituto Italiano di Tecnologia, Centre for Biomolecular Nanotechnologies, Via Barsanti 14, Lecce 73010, Italy

*Corresponding authors: salvatore.gambino@nanotec.cnr.it; agostina.capodilupo@nanotec.cnr.it

Table of contents

1. Materials' optical and structural properties

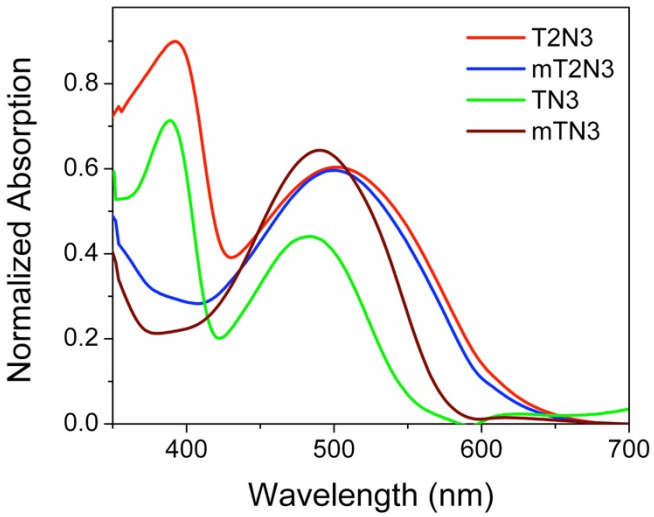

Figure S1. UV-Vis solid state absorption spectra.

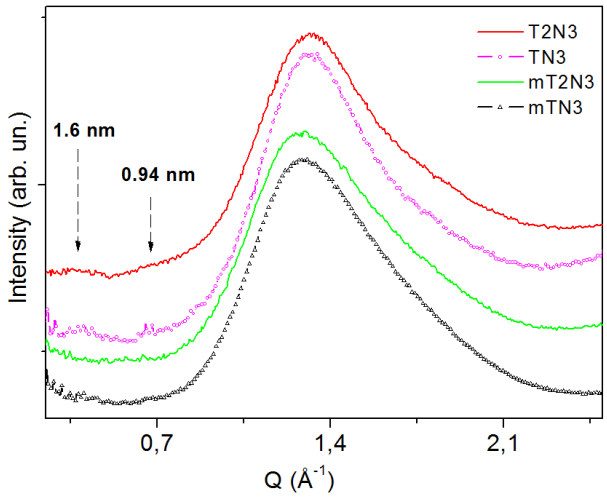

Figure S2. 1D-folded GIWAXS patterns collected at 87 mm sample-detector distance from HTM thin films. The two weak peaks corresponding to nanoscale periodicities of 1.60 ± 0.05 nm and 0.94 ± 0.05 nm are indicated by arrows, which can be clearly recognized in T2N3 and TN3 samples but are hardly visible in mT2N3 and mTN3 samples for such a relatively short integration time (~ 50 min).

2. Room temperature SCLC and conductivity measurements

The current−voltage (J−V) characteristics of each material was recorded under the same experimental conditions, such as in dark, in vacuum (10^{-2} mbar) and at a controlled temperature. Figure S3a shows room temperature J-V curves in semi-log scale (symbols), which clearly show that under the same bias condition the current density is higher for materials whose arylamino moieties are anchored on the 2,7-position of DBF (**TN3**, **T2N3**), than to those having them on the 3,6-position of DBF (**mTN3**, **mT2N3**). Furthermore, within the same group, molecules containing two thiophene units (**T2**) show a higher current density.

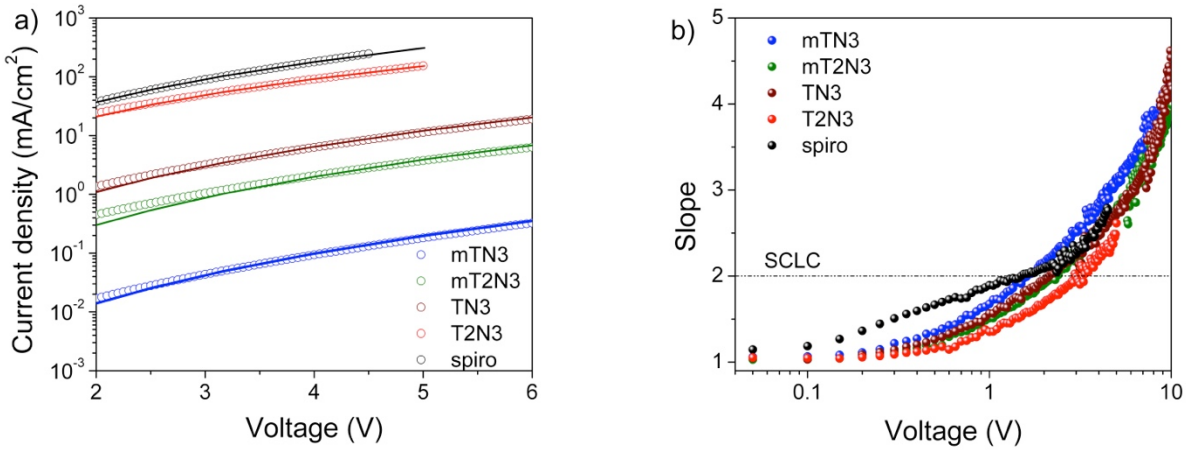

Figure S3. Room temperature current versus voltage (a) and the corresponding slope versus voltage (b) of hole-only devices. Experimental data (symbols) were fitted according to equation 1 in the main text (solid lines).

The calculated slopes in Figure S3b are quite similar, they show an extended ohmic region (slope = 1), which suggests no trapping phenomena (or at least negligible) [1]. At an applied voltage larger than 2 V, charge carriers enter into the so-called space charge regime (slope = 2). However, in the case of disordered systems, such as organic semiconductors, the slope is larger than 2, which is usually ascribed to a Gaussian distribution of hopping sites (DOS), namely energetic disorder (see main text).

From the ohmic region (slope = 1) it was possible to determine the electrical conductivity. Figure S4 gives the conductivity of the four compounds investigated along with the reference sample (spiro), whose conductivity is in very good agreement with Snaith et al. [2] and Hawash et al. [3]. The conductivities (full symbols) show a rather similar trend compared to the mobility (open symbols).

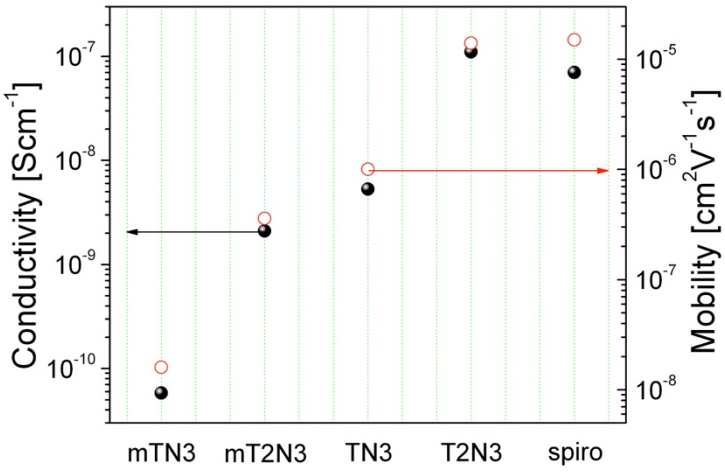

Figure S4. Conductivity (full symbols) and mobility (open symbols) values, extracted from the ohmic and SCLC regions, respectively.

3. Effect of built-in voltage in non-symmetric devices

We have seen in Figure S3b that the slope-voltage characteristics of our molecules did not show any obvious peak, and their shape is similar to the case of a Gaussian disorder without any traps [4]. Our HTMs are sandwiched between two ohmic and symmetric contacts, a bottom transparent conductive oxide ITO/Pedot:PSS and a top metal contact MoO_3/Au. A different choice of contacts would have hindered a "clear" investigation of our HTMs, resulting in an "bump" in the slope curve. Figure S5, indeed, shows the J-V characteristic of compound **TN3**, in the case of a device structure where the top MoO_3/Au contact has been replaced with silver (Ag). In this latter case we recorded an S-shaped J-V curve, which translated into a slope-voltage curve characterized by a clear peak at around 1.5 V, which was actually absent in the MoO_3/Au top contact configuration (Figure S5 inset). Usually a peak in the slope reveal the presence of traps within the bandgap of a semiconductor [1]. However, a similar effect could be induced by the presence of a built-in voltage [5], which can lead to a misleading interpretation of the results. This is, indeed, what happened in the present case once we used asymmetric contacts. This result indicates the importance of good ohmic and symmetric contacts for a correct study of charge transport by the SCLC method.

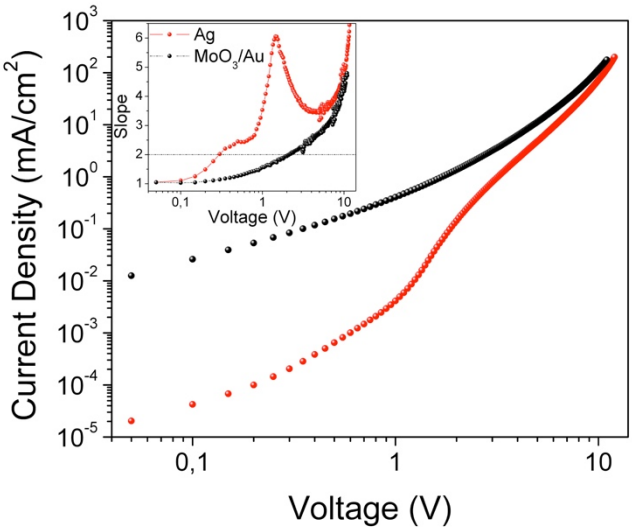

Figure S5. Room temperature current versus voltage characteristics for a **TN3** based hole-only device and slopes against voltage plots (inset). Red dots are the experimental data for the Ag top contact device, meanwhile black dots for the MoO_3/Au. Data have been recorded by applying a positive bias to the ITO.

To further demonstrate, without any doubt, that the "bump" in the slope curve is an effect of the built-in voltage (V_{bi}), we compared, in Figure S6a, the forward and the reverse current density curves of symmetric (black dots) and asymmetric (red dots) hole-only devices. In the case of asymmetric devices, in forward bias, the V_{bi} introduces a barrier for charge-carriers to overcome, whereas in reverse bias the current will be injection limited. The energetic barrier manifests itself by a large peak in the slope-voltage curve, as shown in Figure S6b (open symbols). If the peak was due to trapping phenomena we should see the same large peak also in the slope-voltage characteristic of the reverse biased devices. Clearly this is not the case as shown in Figure S6b (full symbols).

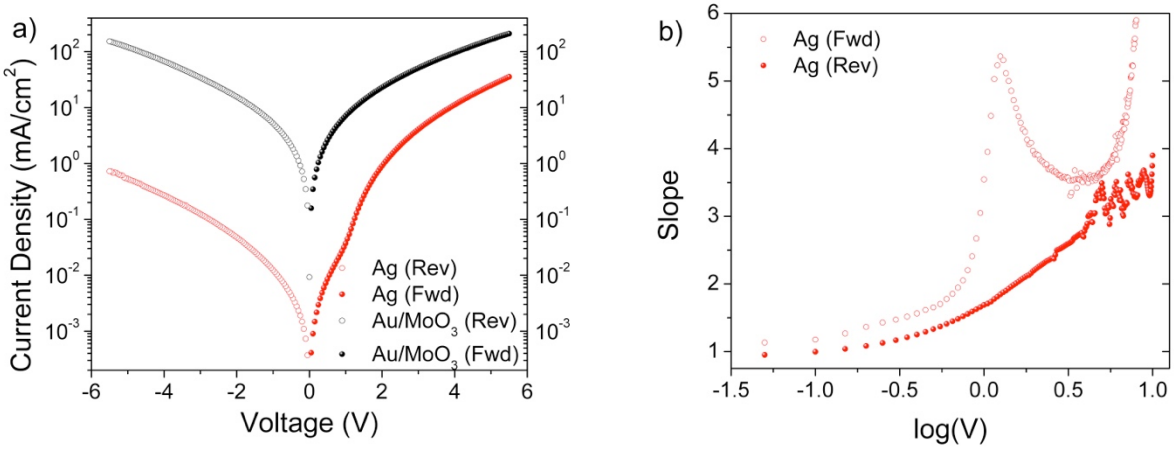

Figure S6. a) Forward (full symbols) and reverse (empty symbols) J-V curves obtained from SCLC measurements of symmetric (black dots) and asymmetric (red dots) **T2N3** hole-only devices. b) slope-voltage plots of the J-V data of asymmetric devices.

4. Drift-Diffusion slope fits and hopping parameters

SCLC measurements are shown in the main text in the form of current-voltage characteristics. Meanwhile, in Figure S7 below are reported the related slope-voltage curves. The slope (m) is defined as follow:

$$m = \frac{dlogJ}{dlogV}$$

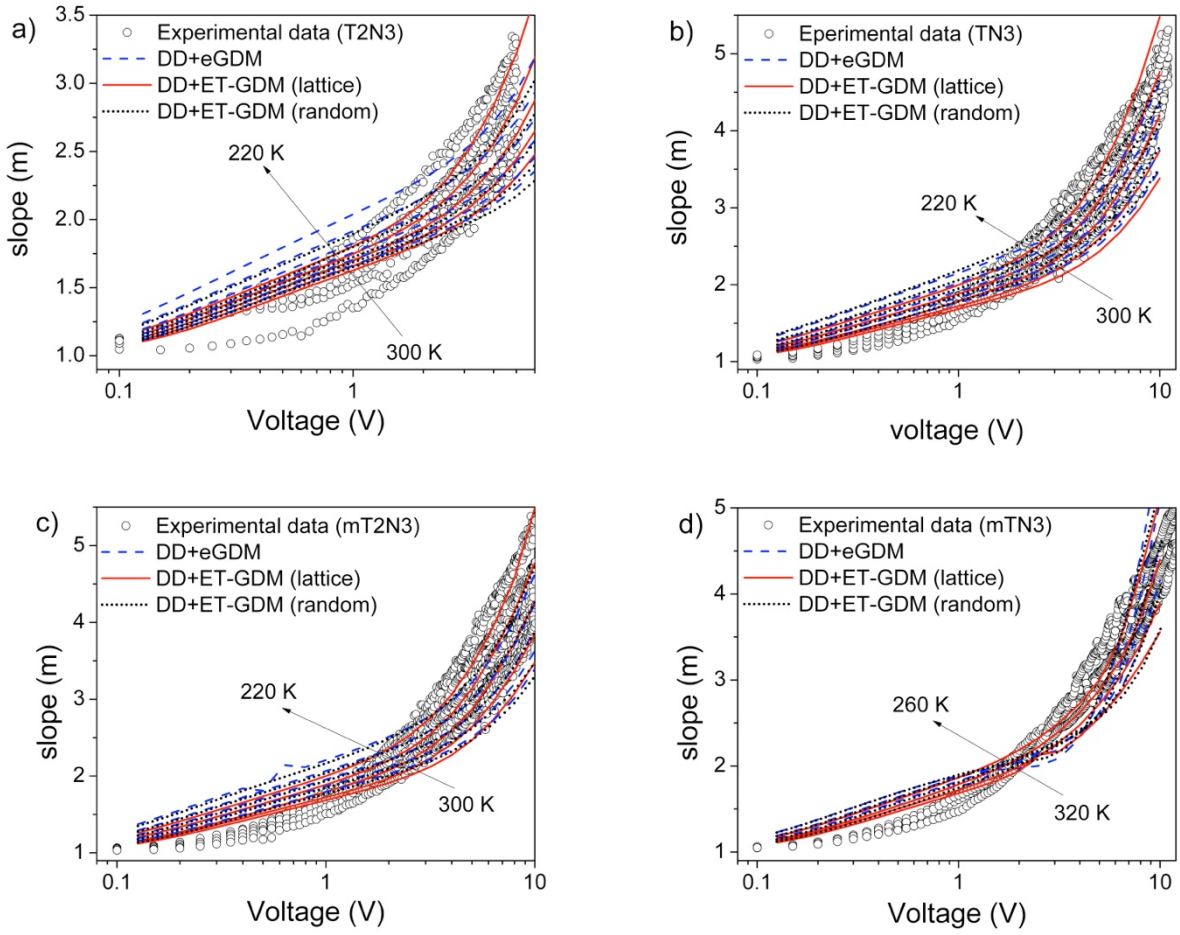

Figure S7. Slope versus voltage characteristics against temperature of a) **T2N3**, b) **TN3**, c) **mT2N3** and d) **mTN3** based hole-only devices. Symbols represent experimental data and lines are numerical drift-diffusion model fits with mobilities described using the eGDM (dashed blue lines), lattice ET-GDM (solid red lines) and random ET-GDM (dotted black lines) models.

MG + GDM								
Materials	σ_{HOMO} [meV]	μ_0 @ 300 K [cm^2/Vs]	γ @ 300 K [V/m]	μ^* [cm^2/Vs]	B $x10^{-5}$	T_0 [K]	Φ_1 [eV]	Φ_2 [eV]
T2N3	89	$3.0*10^{-5}$	$1.45*10^{-4}$	$5*10^{-3}$	2.09	361	0.1	0.3
TN3	97	$8.7*10^{-7}$	$3.9*10^{-4}$	$4.6*10^{-4}$	2.28	535	0.1	0.3
mT2N3	96	$2.4*10^{-7}$	$4.8*10^{-4}$	$8.9*10^{-5}$	2.47	591	0.1	0.3
mTN3	109	$7.0*10^{-9}$	$5.3*10^{-4}$	$2.2*10^{-5}$	2.38	713	0.1	0.3

Table S1. Fitting parameters for hole-only devices of Figure 5 extracted using the MG+GDM model.

DD + eGDM						
Materials	σ_{HOMO} [meV]	μ_0 @ 300 K [cm^2/Vs]	ν_0 [s^{-1}]	α_{NN} [m]	Φ_1 [eV]	Φ_2 [eV]
T2N3	94	$2.6*10^{-5}$	$4.1*10^{10}$	$1.6*10^{-9}$	0.11	0.07
TN3	111	$1.0*10^{-6}$	$1.1*10^{10}$	$2.1*10^{-9}$	0.09	0.10
mT2N3	118	$2.9*10^{-7}$	$1.0*10^{10}$	$2.0*10^{-9}$	0.09	0.09
mTN3	110	$1.2*10^{-8}$	$3.8*10^{7}$	$3.5*10^{-9}$	0.07	0.15

DD + ET-GDM (lattice)								
Materials	σ_{HOMO} [meV]	μ_0 @ 300 K [cm^2/Vs]	α_{NN} [m]	α [m]	ν_0 [s^{-1}]	α_{NN}/α	Φ_1 [eV]	Φ_2 [eV]
T2N3	83	$1.4*10^{-5}$	$1.0*10^{-9}$	$3.7*10^{-10}$	$7.7*10^{9}$	2.7	0.02	0.10
TN3	97	$1.0*10^{-6}$	$1.7*10^{-9}$	$3.6*10^{-10}$	$1.1*10^{9}$	4.6	0.10	0.06
mT2N3	100	$3.6*10^{-7}$	$1.6*10^{-9}$	$4.0*10^{-10}$	$6.2*10^{8}$	3.8	0.10	0.12
mTN3	104	$1.6*10^{-8}$	$1.8*10^{-9}$	$4.6*10^{-10}$	$4.3*10^{7}$	3.9	0.08	0.15

DD + ET GDM (random)								
Materials	σ_{HOMO} [meV]	μ_0 @ 300 K [cm^2/Vs]	α_{NN} [m]	α [m]	ν_0 [s^{-1}]	α_{NN}/α	Φ_1	Φ_2
T2N3	87	$2.95*10^{-5}$	$2.2*10^{-9}$	$2.4*10^{-10}$	$1.4*10^{10}$	9.2		
TN3	109	$9.47*10^{-7}$	$2.3*10^{-9}$	$4.6*10^{-10}$	$4.6*10^{9}$	5.0		
T2N3	118	$4.0*10^{-7}$	$1.9*10^{-9}$	$3.2*10^{-10}$	$1.8*10^{10}$	5.9		
mTN3	118	$1.7*10^{-8}$	$2.1*10^{-9}$	$5.3*10^{-10}$	$1.6*10^{8}$	3.9		

Table S2. Fitting parameters for hole-only devices of Figure 6. Parameters were estimated using the DD model parametrized according to eGDM, lattice ET-GDM and random ET-GDM models.

5. Perovskite solar cells

Solution cast on top of perovskite films, for solar cell making, led to high quality films but **mT2N3**, which was characterized by a poor-quality film as shown by SEM image (Figure S8). PSCs based on **mT2N3** were highly unreproducible and data were inconsistent not only from sample-to-sample but also within pixels of the same sample. Thus, we dropped **mT2N3** from solar cells characterization.

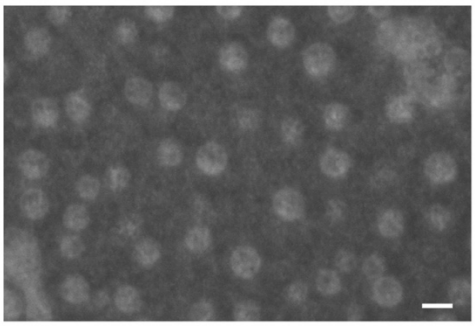

Figure S8. SEM image of an **mT2N3** film on top of a perovskite layer. Scale bar is 1 μm.

Materials	FF [%] Rev Fwd	V_{oc} [V] Rev Fwd	J_{sc} [mA] Rev Fwd	PCE [%] Rev Fwd
Spiro	72 ± 1 71 ± 1	1,08 ± 0,02 1,08 ± 0,02	20,5 ± 0,6 20,5 ± 0,7	15,9 ± 0,7 15,6 ± 0,9
T2N3	71 ± 2 69 ± 2	1,08 ± 0,01 1,07 ± 0,01	20,7 ± 0,5 20 ± 2	15,8 ± 0,6 15 ± 1
TN3	69 ± 2 67 ± 3	1,01 ± 0,03 1,01 ± 0,03	19,0 ± 0,9 18,6 ± 0,8	13,5 ± 0,7 12,5 ± 0,7
mTN3	67 ± 4 66 ± 4	1,00 ± 0,06 1,02 ± 0,05	16 ± 1 16 ± 1	11 ± 1 11 ± 1

Table S3. Solar cell parameters statistical data collected from J-V curves based on different HTMs.

	τ_1 (ns)	τ_2 (ns)	α_1	α_2	τ_{avg} (ns)
MAPI	35.7	140.6	169	746	134.9
MAPI/mTN3	1.5	25.2	827	101	17.5
MAPI/T2N3	2.2	23.3	678	177	17.7
MAPI/spiro	2.5	23.7	706	198	17.9
MAPI/TN3	1.9	22.0	709	173	16.3

Table S4. Fitted decay lifetimes and corresponding pre-exponential factors of a neat perovskite film (MAPI) and MAPI/HTMs samples.

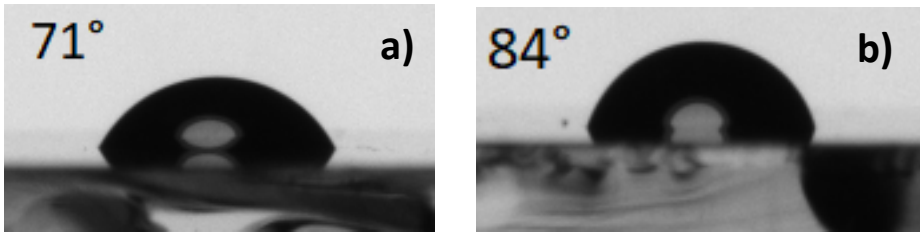

Figure S9. Water contact angles of a) spiro and b) **T2N3** doped thin films.

References:

[1] G. Zuo, Z. Li, O. Andersson, H. Abdalla, E. Wang, M. Kemerink, Molecular Doping and Trap Filling in Organic Semiconductor Host–Guest Systems, J. Phys. Chem. C. 121 (2017) 7767–7775. https://doi.org/10.1021/acs.jpcc.7b01758.

[2] H.J. Snaith, M. Grätzel, Enhanced charge mobility in a molecular hole transporter via addition of redox inactive ionic dopant: Implication to dye-sensitized solar cells, Appl. Phys. Lett. 89 (2006) 262114. https://doi.org/10.1063/1.2424552.

[3] Z. Hawash, L.K. Ono, Y. Qi, Moisture and Oxygen Enhance Conductivity of LiTFSI-Doped Spiro-MeOTAD Hole Transport Layer in Perovskite Solar Cells, Adv. Mater. Interfaces. 3 (2016) 1600117. https://doi.org/10.1002/admi.201600117.

[4] N. Felekidis, A. Melianas, M. Kemerink, Automated open-source software for charge transport analysis in single-carrier organic semiconductor diodes, Org. Electron. 61 (2018) 318–328. https://doi.org/10.1016/j.orgel.2018.06.010.

[5] G. Zuo, M. Linares, T. Upreti, M. Kemerink, General rule for the energy of water-induced traps in organic semiconductors, Nat. Mater. 18 (2019) 588–593. https://doi.org/10.1038/s41563-019-0347-y.